Analytical Prediction of Electromagnetic Performances and Unbalanced Magnetic Forces in Fractional-Slot Spoke-Type Permanent-Magnet Machines

K. Boughrara, R. Ibtiouen, F. Dubas

Abstract -- **This paper presents an analytical method for the computation of electromagnetic performances and non-intrinsic unbalanced magnetic forces (UMF) in fractional-slot spoke-type permanent-magnet (STPM) machines. It is based on the two-dimensional (2-D) subdomain method in polar coordinates considering the drive current: i) sinusoidal, and ii) six-step rectangular. It involves solution of Laplace's and Poisson's equations in the stator slots, the air-gap, the buried tangential PMs into rotor slots, and the non-magnetic region under PMs. The results obtained with 2-D analytical model (viz., the electromagnetic performances and the non-intrinsic UMF) are verified with those issued from finite-element method (Fem).**

Index Terms--**Electromagnetic performances, fractional-slot machines, subdomain method, unbalanced magnetic forces.**

I. Introduction

THE STPM STPM machines represent a good candidate for replacing surface-mounted PM (SMPM) machines. This type of machines has a salient rotor in comparison with smooth rotor SMPM machines. The structure of rotor, the number of stator slots, and the number of rotor poles can produce the non-intrinsic UMF [1]-[9]. The intrinsic UMF are generated by the static/dynamic rotor eccentricities or uneven distribution of material properties [9]-[11]. Many authors have analyzed analytically the magnetic field, the electromagnetic performances and UMF in SMPM machines [2]-[7]. However, in our best knowledge the analytical calculation of magnetic field, electromagnetic performances and UMF in fractional-slot STPM machines has not been done. Only integer-slot machines have been analyzed analytically in [12]-[13]. Moreover, UMF in SMPM is generally predicted with using air-gap permeance functions [8]-[9]. However, there is no permeance function that can represent accurately the rotor saliency with the concentrating effect and the stator slots for STPM machines. Generally, the numerical methods can provide a high accuracy for predicting magnetic field and UMF in any number of slot/pole combinations of STPM machines [1] and [14]. But usually require a long computing time.

In this paper, an analytical prediction of magnetic field distribution, electromagnetic performances and non-intrinsic UMF in fractional-slot STPM machines is presented. The analytical magnetic field distribution is computed in polar coordinates from 2-D subdomain method (i.e., based on formal resolution of Maxwell's equations applied in subdomain) in each region, i.e. stator slots, air-gap, buried PMs into rotor slots, and non magnetic region under PMs. The PMs are tangentially magnetized (in order to improve air-gap flux density by flux focusing). This model with single layer winding is valid for any number of slot/pole combinations and can be extended easily for double layer winding. The 2-D analytical results considering the drive current (i.e., sinusoidal and six-step rectangular current) are compared with those obtained by 2-D Fem [16]. The comparisons (viz., the electromagnetic performances and the non-intrinsic UMF) are very satisfying in amplitudes and waveforms.

II. Studied Machine and Magnetic Field Solution

A. Problem Description and Assumptions

Fig. 1 shows the fractional-slot STPM machine where Region I represents the air-gap, Region II the buried PMs, Regions III the stator slots, Region IV the non-magnetic material under PMs. The 2-D analytical model is formulated in magnetic vector potential and polar coordinates with the following assumptions:

- The axial length of the machine is infinite and invariant (i.e., end-effects are neglected);
- The iron parts are assumed to be infinitely permeable;
- The rotor and stator tooth-tips are not considered. However, they can be introduced easily;
- The current density in the stator slots has only one component along the *z*-axis;
- The stator and rotor slots have radial sides;
- Eddy-current effects in the stator winding and in the buried PMs are neglected;
- The PMs demagnetization curve is assumed to be linear;
- The direction of PMs magnetization is supposed purely tangential, i.e., $\overrightarrow{M} = \{0, M_\theta, 0\}$.

The partial differential equations for magnetic fields in each region can be expressed by

$$\nabla^2 A_z = 0 \text{ in Region I and IV (}\textit{Laplace's equation}\text{)} \quad (1)$$

$$\nabla^2 A_z = -\mu_0 \cdot \nabla \times \overrightarrow{M} \text{ in Region II (}\textit{Poisson's equation}\text{)} \quad (2)$$

$$\nabla^2 A_z = -\mu_0 \cdot J_z \text{ in Region III (}\textit{Poisson's equation}\text{)} \quad (3)$$

where $\overrightarrow{M}$ is the PMs magnetization, J_z the current density in the stator slots, and μ_0 the vacuum permeability.

K. Boughrara and R. Ibtiouen are with Ecole National Polytechnique (LRE-ENP: http://www.enp.edu.dz/), 10 av. Pasteur, El-Harrach, BP182, 16200 Algiers, Algeria (e-mail: kamel.boughrara@g.enp.edu.dz, rachid.ibtiouen@gmail.com).

F. Dubas is with the ENERGY Department, FEMTO-ST Institute (http://www.femto-st.fr/), UMRC CNRS 6174, UBFC, Belfort, France (e-mail: FDubas@gmail.com).

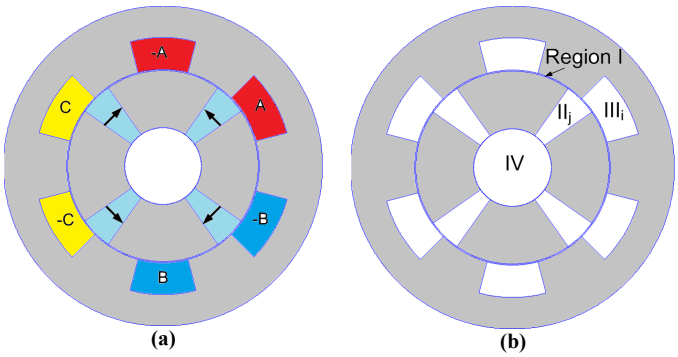

Fig. 1. Studied machine: **(a)** Fractional-slot STPM machine (6-slots/4-poles) with the buried PMs and the single layer winding (i.e., non-overlapping alternate teeth wound winding), and **(b)** Definition of regions for the analytical model.

The field vectors $\vec{B}=\{B_r;B_\theta;0\}$ and $\vec{H}=\{H_r;H_\theta;0\}$ are coupled by the following relations (i.e., the magnetic material equation):

$$\vec{B}=\mu_0\cdot\vec{H} \quad \text{in Region I, III, and IV} \tag{4}$$

$$\vec{B}=\mu_0\cdot\mu_r\cdot\vec{H}+\mu_0\cdot\vec{M} \quad \text{in Region II,} \tag{5}$$

where μ_r is the relative magnetic permeability of PMs. Using $\vec{B}=\nabla\times\vec{A}$, the r- and θ-components of magnetic flux density are deduced from A_z by

$$B_r=\frac{1}{r}\cdot\frac{\partial A_z}{\partial\theta} \text{ and } B_\theta=-\frac{\partial A_z}{\partial r} \tag{6}$$

B. Stator Slots (Region III)

In each slot subdomain (i) of Region III, we have to solve (3), i.e., Poisson's equation,

$$\frac{\partial^2 A_{zIIIi}}{\partial r^2}+\frac{1}{r}\cdot\frac{\partial A_{zIIIi}}{\partial r}+\frac{1}{r^2}\cdot\frac{\partial^2 A_{zIIIi}}{\partial\theta^2}=-\mu_0\cdot J_{zi} \tag{7}$$

where J_{zi} is the current density in the i^{th} stator slot.

The i^{th} stator slot subdomain (called region III), where i vary from 1 to Q_s with Q_s the number of stator slots, is associated with boundary conditions at the bottom and at each sides of the slot [12]-[13].

Using the method of separation of variables, (7) becomes

$$A_{zIIIi}=\begin{vmatrix} C_{i,0}+\frac{1}{2}\mu_0\cdot J_{zi}\cdot\left(r_4^2\ln(r)-\frac{1}{2}r^2\right) \\ +\sum_{m=1}^{\infty}C_{i,m}\cdot f_m(r)\cdot\cos\left[\frac{m\pi}{c}\cdot\left(\theta-\alpha_i+\frac{c}{2}\right)\right]\end{vmatrix} \tag{8a}$$

$$f_m(r)=r^{-\frac{m\pi}{c}}+r_4^{-\frac{2m\pi}{c}}r^{\frac{m\pi}{c}} \tag{8b}$$

where m is a positive integer, α_i the angular position of the i^{th} stator slot, and c the stator slot-opening.

C. Buried PMs (Region II)

In each buried PM subdomain (j) of Region II, we have to solve (2), i.e., Poisson's equation. Because the direction of PMs magnetization is purely tangential. (2) can be reduced to

$$\frac{\partial^2 A_{zIIj}}{\partial r^2}+\frac{1}{r}\cdot\frac{\partial A_{zIIj}}{\partial r}+\frac{1}{r^2}\cdot\frac{\partial^2 A_{zIIj}}{\partial\theta^2}=-\mu_0\cdot\frac{M_\theta}{r} \tag{9}$$

where $M_\theta=M_j=(-1)^j\cdot B_{rm}/\mu_0$ with j varying from 1 to $2p$ poles and B_{rm} the remanent flux density of PMs.

Using the method of separation of variables, (9) becomes

$$A_{zIIj}=\begin{vmatrix} A5_{j,0}+A6_{j,0}\cdot\ln(r)-\mu_0\cdot M_j\cdot r \\ +\sum_{k=1}^{\infty}\begin{pmatrix} A5_{j,k}\cdot r^{-\frac{k\pi}{a}} \\ +A6_{j,k}\cdot r^{\frac{k\pi}{a}}\end{pmatrix}\cdot\cos\left[\frac{k\pi}{a}\cdot\left(\theta-g_j+\frac{a}{2}\right)\right]\end{vmatrix} \tag{10}$$

where k is a positive integer, g_j the angular position of the j^{th} PM, and a the PM-opening.

D. Air-gap (Region I)

In the air-gap (which is an annular domain), we have to solve (1), i.e., Laplace's equation,

$$\frac{\partial^2 A_{zI}}{\partial r^2}+\frac{1}{r}\cdot\frac{\partial A_{zI}}{\partial r}+\frac{1}{r^2}\cdot\frac{\partial^2 A_{zI}}{\partial\theta^2}=0 \tag{11}$$

Using the method of separation of variables, and taking into account the periodicity boundary condition between 0 and 2π for the studied machine with fractional-slot winding, (11) becomes

$$A_{zI}=\begin{vmatrix} A1_0+A2_0\cdot\ln(r) \\ +\sum_{n=1}^{\infty}\left[\begin{matrix}\left(A1_n\cdot r^n+A2_n\cdot r^{-n}\right)\sin(n\theta) \\ +\left(A3_n\cdot r^n+A4_n\cdot r^{-n}\right)\cos(n\theta)\end{matrix}\right]\end{vmatrix} \tag{12}$$

where n is a positive integer.

E. Non-magnetic material under PMs (Region IV)

In the no-magnetic material under PMs (which is an circular domain), we have to solve (1), i.e., Laplace's equation,

$$\frac{\partial^2 A_{zIV}}{\partial r^2}+\frac{1}{r}\cdot\frac{\partial A_{zIV}}{\partial r}+\frac{1}{r^2}\cdot\frac{\partial^2 A_{zIV}}{\partial\theta^2}=0 \tag{13}$$

Using the method of separation of variables, and taking

into account the periodicity boundary condition between *0* and 2π as well as the finite value of the magnetic vector potential at $r = 0$, (13) becomes

$$A_{zIV} = \sum_{n=1}^{\infty} r^n \cdot \left[A7_n \cdot \sin(n\theta) + A8_n \cdot \cos(n\theta) \right] \tag{14}$$

III. Interface Conditions Between Regions

To determine the integration constants in (8), (10), (12) and (14); the boundary conditions at the interface between the various regions should be introduced. This boundary conditions are

- between Region II/Region IV at $r = R_r$:

$$A_{zIIj} = A_{zIV} \ \ for\ \theta \in \left[g_j - a/2, g_j + a/2 \right] \tag{15}$$

$$H_{\theta IV} = \begin{cases} H_{\theta IIj} \ \ for\ \theta \in \left[g_j - a/2, g_j + a/2 \right] \\ 0 \ otherwise \end{cases} \tag{16}$$

- between Region II/Region I at $r = R_m$:

$$A_{zIIj} = A_{zI} \ \ for\ \theta \in \left[g_j - a/2, g_j + a/2 \right] \tag{17}$$

$$H_{\theta I} = \begin{cases} H_{\theta IIj} \ \ for\ \theta \in \left[g_j - a/2, g_j + a/2 \right] \\ 0 \ otherwise \end{cases} \tag{18}$$

- between Region III/Region I at $r = R_s$:

$$A_{zIIIi} = A_{zI} \ \ for\ \theta \in \left[\alpha_i - c/2, \alpha_i + c/2 \right] \tag{19}$$

$$H_{\theta I} = \begin{cases} H_{\theta IIIi} \ \ for\ \theta \in \left[\alpha_i - c/2, \alpha_i + c/2 \right] \\ 0 \ otherwise \end{cases} \tag{20}$$

The interface conditions (15) ~ (20) concern regions with different subdomain frequencies which need Fourier series expansions to satisfy equalities of magnetic vector potential and field at each interface radius.

According to Fourier series expansion, the interface condition (15) gives

$$\begin{aligned} & A5_{j,0} + A6_{j,0} \cdot \ln(R_r) - \mu_0 \cdot M_j \cdot R_r \\ &= \frac{1}{a} \cdot \int_{g_j - \frac{a}{2}}^{g_j + \frac{a}{2}} A_{zIV}\big|_{r=R_r} \cdot d\theta \end{aligned} \tag{21}$$

$$\begin{aligned} & A5_{j,k} \cdot R_r^{-k\pi/a} + A6_{j,k} \cdot R_r^{k\pi/a} \\ &= \frac{2}{a} \cdot \int_{g_j - \frac{a}{2}}^{g_j + \frac{a}{2}} A_{zIV}\big|_{r=R_r} \cdot \cos\left[\frac{k\pi}{a} \cdot \left(\theta - g_j + \frac{a}{2} \right) \right] \cdot d\theta \end{aligned} \tag{22}$$

(16) gives

$$\begin{aligned} & -\frac{n}{\mu_0} \cdot A7_n \cdot R_r^{n-1} \\ &= \frac{1}{\pi} \cdot \sum_{j=1}^{2p} \int_{g_j - \frac{a}{2}}^{g_j + \frac{a}{2}} H_{\theta IIj}\big|_{r=R_r} \cdot \sin(n\theta) \cdot d\theta \end{aligned} \tag{23}$$

$$\begin{aligned} & -\frac{n}{\mu_0} \cdot A8_n \cdot R_r^{n-1} \\ &= \frac{1}{\pi} \cdot \sum_{j=1}^{2p} \int_{g_j - \frac{a}{2}}^{g_j + \frac{a}{2}} H_{\theta IIj}\big|_{r=R_r} \cdot \cos(n\theta) \cdot d\theta \end{aligned} \tag{24}$$

(17) gives

$$\begin{aligned} & A5_{j,0} + A6_{j,0} \cdot \ln(R_m) - \mu_0 \cdot M_j \cdot R_m \\ &= \frac{1}{a} \cdot \int_{g_j - \frac{a}{2}}^{g_j + \frac{a}{2}} A_{zI}\big|_{r=R_m} \cdot d\theta \end{aligned} \tag{25}$$

$$\begin{aligned} & A5_{j,k} \cdot R_m^{-k\pi/a} + A6_{j,k} \cdot R_m^{k\pi/a} \\ &= \frac{2}{a} \cdot \int_{g_j - \frac{a}{2}}^{g_j + \frac{a}{2}} A_{zI}\big|_{r=R_m} \cdot \cos\left[\frac{k\pi}{a} \cdot \left(\theta - g_j + \frac{a}{2} \right) \right] \cdot d\theta \end{aligned} \tag{26}$$

(18) gives

$$-\frac{A2_0}{\mu_0 R_m} = \frac{1}{a} \cdot \sum_{j=1}^{2p} \int_{g_j - \frac{a}{2}}^{g_j + \frac{a}{2}} H_{\theta IIj}\big|_{r=R_m} \cdot d\theta \tag{27}$$

$$\begin{aligned} & -\frac{n}{\mu_0} \cdot \left(A1_n \cdot R_m^{n-1} - A2_n \cdot R_m^{-n-1} \right) \\ &= \frac{1}{\pi} \cdot \sum_{j=1}^{2p} \int_{g_j - \frac{a}{2}}^{g_j + \frac{a}{2}} H_{\theta IIj}\big|_{r=R_m} \cdot \sin(n\theta) \cdot d\theta \end{aligned} \tag{28}$$

$$\begin{aligned} & -\frac{n}{\mu_0} \left(A3_n \cdot R_m^{n-1} - A4_n \cdot R_m^{-n-1} \right) \\ &= \frac{1}{\pi} \cdot \sum_{j=1}^{2p} \int_{g_j - \frac{a}{2}}^{g_j + \frac{a}{2}} H_{\theta IIj}\big|_{r=R_m} \cdot \cos(n\theta) \cdot d\theta \end{aligned} \tag{29}$$

(19) gives

$$C_{i,0}+\frac{1}{2}\mu_0\cdot J_{zi}\cdot\left(r_4{}^2\cdot\ln\left(R_s\right)-\frac{1}{2}\cdot R_s^2\right)=\frac{1}{c}\cdot\int_{\alpha_i-\frac{c}{2}}^{\alpha_i+\frac{c}{2}}A_{zI}\big|_{r=R_s}\cdot d\theta \tag{30}$$

$$C_{i,m}\cdot\left(R_s{}^{-m\pi/c}+r_4{}^{-2m\pi/c}\cdot R_s{}^{m\pi/c}\right)=\frac{2}{c}\cdot\int_{\alpha_i-\frac{c}{2}}^{\alpha_i+\frac{c}{2}}A_{zI}\big|_{r=R_s}\cdot\cos\left[\frac{m\pi}{c}\cdot\left(\theta-\alpha_i+\frac{c}{2}\right)\right]\cdot d\theta \tag{31}$$

and (20) gives

$$-\frac{1}{\mu_0}\cdot\frac{A2_0}{R_s}=\frac{1}{2\pi}\cdot\sum_{i=1}^{Q_s}\int_{\alpha_i-\frac{c}{2}}^{\alpha_i+\frac{c}{2}}H_{\theta IIIi}\big|_{r=R_s}\cdot d\theta \tag{32}$$

$$-\frac{n}{\mu_0}\cdot\left(A1_n\cdot R_s^{n-1}-A2_n\cdot R_s^{-n-1}\right)=\frac{1}{\pi}\cdot\sum_{i=1}^{Q_s}\int_{\alpha_i-\frac{c}{2}}^{\alpha_i+\frac{c}{2}}H_{\theta IIIi}\big|_{r=R_s}\cdot\sin\left(n\theta\right)\cdot d\theta \tag{33}$$

$$-\frac{n}{\mu_0}\cdot\left(A3_n\cdot R_s{}^{n-1}-A4_n\cdot R_s{}^{-n-1}\right)=\frac{1}{\pi}\cdot\sum_{i=1}^{Q_s}\int_{\alpha_i-\frac{c}{2}}^{\alpha_i+\frac{c}{2}}H_{\theta IIIi}\big|_{r=R_s}\cdot\cos\left(n\theta\right)\cdot d\theta \tag{34}$$

From (21) ~ (34), we can calculate the 14 coefficients by solving a Cramer's systems with a given number of harmonics for *n, k* and *m*.

IV. Calculation of Electromagnetic Performances and UMF

The developed analytical method for fractional-slot STPM machines is used to determine electromagnetic performances and non-intrinsic UMF.

A. Flux Linkage and Back Electromotive Force (EMF)

In order to calculate magnetic field distribution, the current density in the i^{th} stator slots, i.e., J_{zi}, is defined by

$$J_{zi}=\frac{N_c}{S}\cdot C^T\cdot\begin{bmatrix}i_a & i_b & i_c\end{bmatrix} \tag{35}$$

in which C represents the winding connection matrix between *q*-phases of current and the stator slots which is defined by

$$C=\begin{bmatrix}1&-1&0&0&0&0\\0&0&0&0&1&-1\\0&0&1&-1&0&0\end{bmatrix} \tag{36}$$

where $S=c\cdot\left(r_4{}^2-R_s{}^2\right)\big/2$ is the slot area, N_c the number of conductors in the stator slot, and $i_\bullet$ the armature currents of *3*-phases. The studied machine is fed by sinusoidal or six-step rectangular currents [15].

The method based on Stokes theorem is used to determine the magnetic flux linkage and the back-EMF. The magnetic flux linkage is defined by

$$\varphi_i=\frac{Lu}{S}\cdot\int_{\alpha_i-\frac{c}{2}}^{\alpha_i+\frac{c}{2}}\int_{R_s}^{r_4}A_{zIIIi}\cdot r\cdot dr\cdot d\theta \tag{37}$$

By using (8), (37) gives

$$\varphi_i=Lu\cdot C_{i,0}+\varphi_{Jzi} \tag{38a}$$

$$\varphi_{Jzi}=-\frac{\mu_0}{8}\cdot Lu\cdot J_{zi}\frac{\left\{\begin{matrix}R_s^4+\left[2-4\ln\left(R_s\right)\right]\cdot r_4{}^2\cdot R_s{}^2\\+\left[4\ln\left(r_4\right)-3\right]\cdot r_4{}^4\end{matrix}\right\}}{R_s{}^2-r_4{}^2} \tag{38b}$$

It is interesting to note that for the no-load condition (i.e., $J_{zi}=0$) and for both models, the term φ_{Jzi} is null. The phase flux vector is given by

$$\begin{bmatrix}\psi_a\\\psi_b\\\psi_c\end{bmatrix}=N_c\cdot C^T\cdot\begin{bmatrix}\varphi_1 & \varphi_2 & \ldots & \varphi_{Q_s-1} & \varphi_{Q_s}\end{bmatrix} \tag{39}$$

The back-EMF vector of *3*-phases is calculated by

$$\begin{bmatrix}E_a\\E_b\\E_c\end{bmatrix}=\Omega\cdot\frac{d}{d\theta_r}\cdot\begin{bmatrix}\psi_a\\\psi_b\\\psi_c\end{bmatrix} \tag{40}$$

with $\theta_r=\Omega\cdot t$ where Ω is the mechanical pulse of synchronism.

B. Electromagnetic Torque

The electromagnetic torque can be computed from the back-EMF by

$$T_{em}=\left(E_a\cdot i_a+E_b\cdot i_b+E_c\cdot i_c\right)\big/\Omega \tag{41}$$

The cogging torque can be determined by the Maxwell stress tensor, i.e.,

$$T_c = \frac{2p \cdot Lu \cdot {R_g}^2}{\mu_0} \cdot \int_0^{\pi/p} B_{rI}\big|_{r=R_g} \cdot B_{\theta I}\big|_{r=R_g} \cdot d\theta \qquad (42)$$

where R_g is the radius of a circle placed at the middle of the air-gap, Lu is the effective axial length of the machine. It should be noted that (42) can also be used to predict electromagnetic torque if the open-circuit flux density is substituted by the on-load flux density.

C. Non-intrinsic UMF

The r- and θ-components of magnetic pressures (in function of θ_r and θ) at R_g are defined as [10]

$$P_r = \frac{1}{2\mu_0} \cdot \left(B_{rI}\big|_{r=R_g}^{\ 2} - B_{\theta I}\big|_{r=R_g}^{\ 2} \right) \qquad (43)$$

$$P_\theta = \frac{1}{\mu_0} \cdot B_{rI}\big|_{r=R_g} \cdot B_{\theta I}\big|_{r=R_g} \qquad (44)$$

The x- and y-components of non-intrinsic UMF at R_g is calculated as [3] and [7]

$$F_x = \frac{R_g \cdot L_u}{2\mu_0} \cdot \int_0^{2\pi} \begin{bmatrix} \left(B_{\theta I}\big|_{r=R_g}^{\ 2} - B_{rI}\big|_{r=R_g}^{\ 2} \right) \cdot \cos(\theta) \\ +2 \cdot B_{\theta I}\big|_{r=R_g} \cdot B_{rI}\big|_{r=R_g} \cdot \sin(\theta) \end{bmatrix} \cdot d\theta \qquad (45)$$

$$F_y = \frac{R_g \cdot L_u}{2\mu_0} \cdot \int_0^{2\pi} \begin{bmatrix} \left(B_{\theta I}\big|_{r=R_g}^{\ 2} - B_{rI}\big|_{r=R_g}^{\ 2} \right) \cdot \sin(\theta) \\ -2 \cdot B_{\theta I}\big|_{r=R_g} \cdot B_{rI}\big|_{r=R_g} \cdot \cos(\theta) \end{bmatrix} \cdot d\theta \qquad (46)$$

V. Analytical Results and Fem Validation

The main dimensions and parameters of the fractional-slot STPM machine (6-slots/4-poles) with the buried PMs and a single layer winding (i.e., non-overlapping alternate teeth wound winding) are given in Table I. Then, analytical results are verified by 2-D Fem [16].

Fig. 2 shows that the flux lines are not equilibrate in each part of the machine in the case of rectangular drive currents. This can be also confirmed in Fig. 3, where radial and tangential flux densities have a periodicity equal to 2π. Figs 4 ~ 6 show the bach-EMF, electromagnetic torque (for both drive currents) and cogging torque curves. We can see in the spectrum of back-EMF [see Fig. 4.b] that the odd harmonics orders 1, 5, 7 and 10 are predominates. For cogging torque spectrum, even harmonics orders 2, 4, 8, and 10 are significant. The radial and tangential magnetic pressures of the brushless DC machine in function of space angle and motion are shown in Figs. 7 and 8. The forces F_x and F_y for both drive currents are shown in Figs. 9 ~ 13. It is clear that the fractionnal-slot STPM machine fed by the six-step rectangular current has more non-intrinsic UMF low harmonics than the fractionnal-slot STPM machine fed by the sinusoidal current even if the torque ripple is lower.

TABLE I
Parameters of Fractional-Slot STPM Machine

Parameters	Value & unit
Remanent flux density of PMs, B_{rm}	0.4 T
Relative permeability of PMs, μ_{rm}	1
Number of conductors per stator slot, N_c	60
Peak phase current, I_m	15 A
Number of stator slots, Q_s	6
Stator slot-opening, c	30°
PM-opening, a	20°
Number of pole pairs, p	2
Radius of the external stator surface, R_o	75 mm
Outer radius of stator slot, r_4	50.3 mm
Radius of the stator outer surface, R_s	45.3 mm
Radius of the rotor inner surface at the PM surface, R_m	44.8 mm
Radius of the rotor inner surface at the PM bottom, R_r	18 mm
Air-gap length, g	0.5 mm
Height of a PM, h_m	26.8 mm
Height of stator slot, h_s	15 mm
Axial length of the machine, L_u	57 mm
Mechanical pulse of synchronism, Ω	157 rad/s

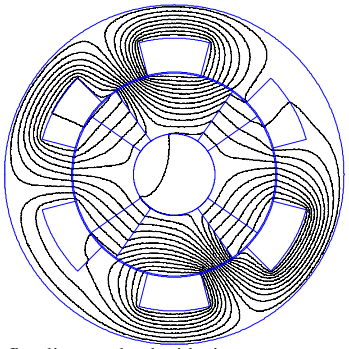

Fig. 2. Fem flux lines on load with six-step rectangular currents.

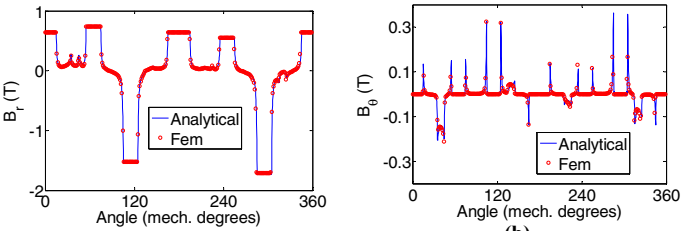

Fig. 3. Flux density on load with six-step rectangular currents: **(a)** Radial, and **(b)** Tangential.

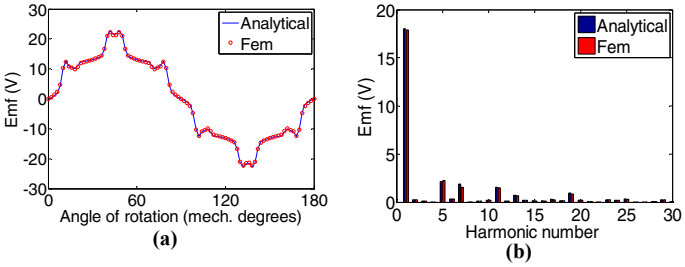

Fig. 4. Back-EMF: **(a)** Waveform, and **(b)** Harmonic spectrum.

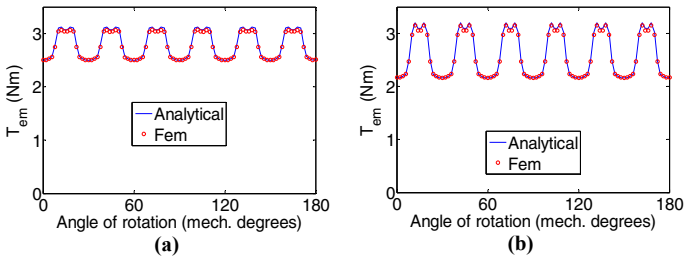

Fig. 5. Electromagnetic torque with **(a)** six-step rectangular, and **(b)** sinusoidal currents.

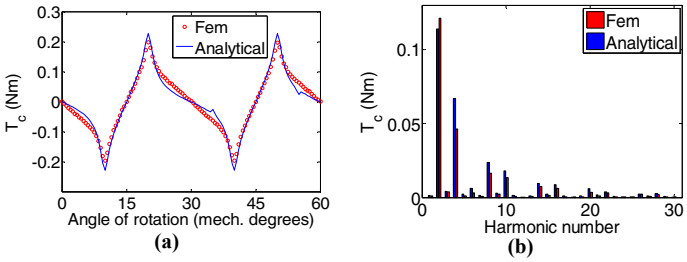

Fig. 6. Cogging torque: **(a)** Waveform, and **(b)** Harmonic spectrum.

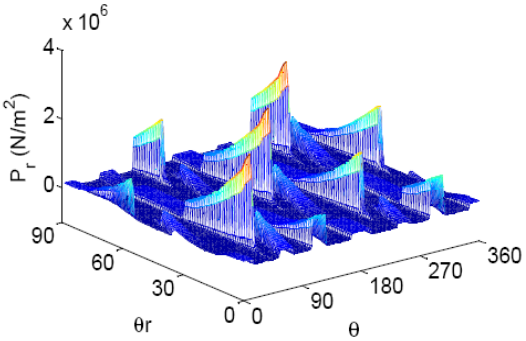

Fig. 7. Analytical radial magnetic pressure on load with six-step rectangular currents versus θ_r and θ.

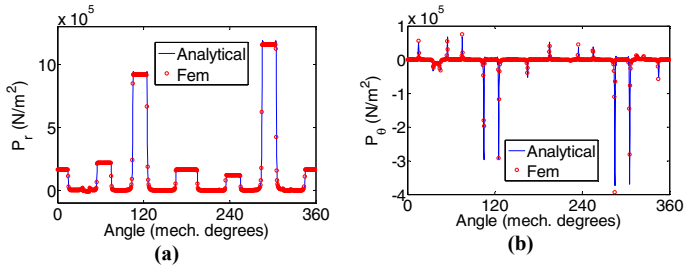

Fig. 8. Magnetic pressures on load with six-step rectangular currents: **(a)** Radial, and **(b)** Tangential.

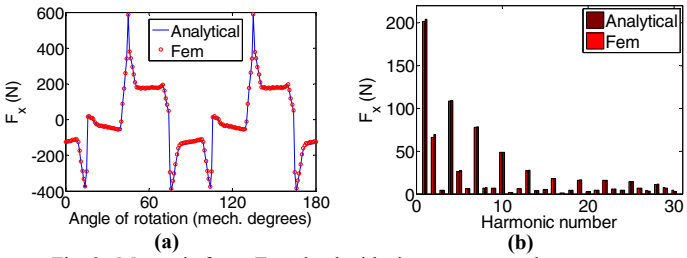

Fig. 9. Magnetic force F_x on load with six-step rectangular currents: **(a)** Waveform, and **(b)** Harmonic spectrum.

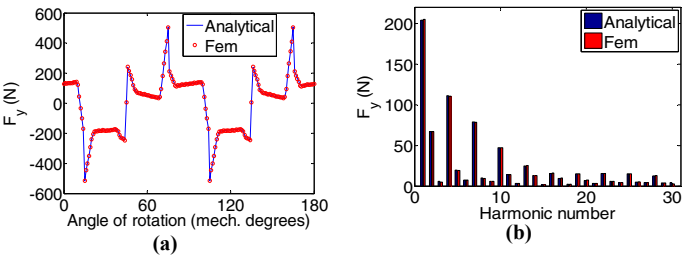

Fig. 10. Magnetic force F_y on load with six-step rectangular currents: **(a)** Waveform, and **(b)** Harmonic spectrum.

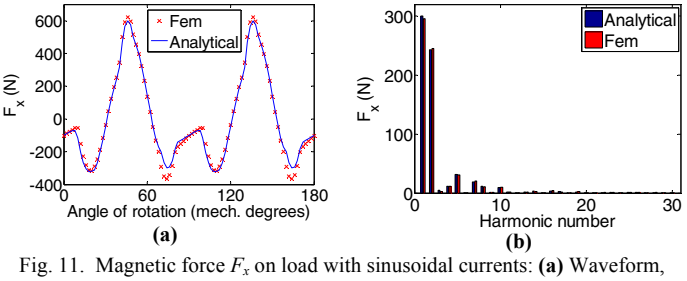

Fig. 11. Magnetic force F_x on load with sinusoidal currents: **(a)** Waveform, and **(b)** Harmonic spectrum.

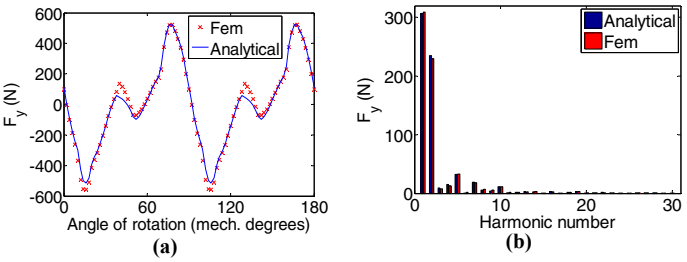

Fig. 12. Magnetic force F_y on load with sinusoidal currents: **(a)** Waveform, and **(b)** Harmonic spectrum.

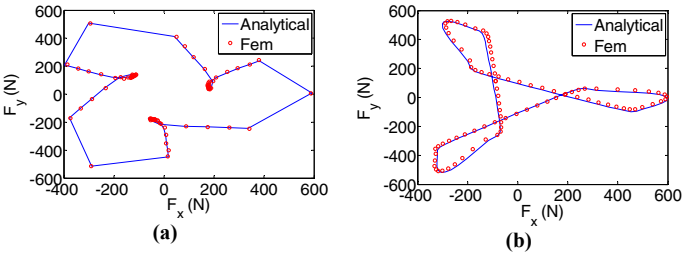

Fig. 13. Locus of the non-intrinsic UMF on load with **(a)** six-step rectangular, and **(b)** sinusoidal currents.

I. Conclusion

In this paper, we have proposed an improved analytical subdomain model for predicting magnetic field distribution, electromagnetic performances and non-intrinsic UMF in the fractional-slot STPM machines (6-slots/4-poles) with the buried PMs and a single layer winding (i.e., non-overlapping alternate teeth wound winding). Poisson's and Laplace's equations are solved analytically using the method of separation of variables in each region. Two types of drive currents are considered (viz., sinusoidal and six-step rectangular currents) to show their effect on the electromagnetic torque and non-intrinsic UMF. Moreover, torque ripple analysis, the spectrum of cogging torque and UMF permit to study the effect of each harmonic on vibration of this type of machines. It is important to notice that the developed analytical method is also valid for any

number of slot/pole combinations, integer and fractional slot and single and double layer winding. Analytical results are in very good agreement with the ones obtained by Fem.

II. References

[1] Y.S. Chen, Z.Q. Zhu and D. Howe, "Vibration of PM Brushless Machines Having a Fractional Number of Slots Per Pole", *IEEE Trans. on Magn.*, vol. 42, no. 10, pp. 3395-3397, October 2006.

[2] L.J. Wu, Z.Q. Zhu, J.T. Chen and Z.P. Xia, "An Analytical Model of Unbalanced Magnetic Force in Fractional-Slot Surface-Mounted Permanent Magnet Machines", *IEEE Trans. on Magn.*, vol. 46, no. 7, pp. 2686-2700, July 2010.

[3] Z.Q. Zhu, D. Ishak, D. Howe and J. Chen, "Unbalanced Magnetic Forces in Permanent-Magnet Brushless Machines With Diametrically Asymmetric Phase Windings", *IEEE Trans. on Industry App.*, vol. 43, no. 6, pp. 1544-1553, November/December 2007.

[4] Z.Q. Zhu, Z.P. Xia, L.J. Wu and G.W. Jewell, "Analytical modeling and finite-element computation of radial vibration force in fractional-slot permanent-magnet brushless machines", *IEEE Trans. on Industry App.*, vol. 46, no. 5, pp. 1908-1918, September/October 2010.

[5] H.C.M. Mai, R. Bernard, P. Bigot, F. Dubas, D. Chamagne, and C. Espanet, "Consideration of Radial Magnetic Forces in Brushless DC Motors", International Conference on Electrical Machines and Systems (ICEMS), pp. 998-1003, October 2010.

[6] H.J. Shin, J.Y. Choi, H.I. Park and S.M. Jang, "Vibration analysis and measurements through prediction of electromagnetic vibration sources of permanent magnet synchronous motor based on analytical magnetic field calculations", *IEEE Trans. on Magn.*, vol. 48, no. 11, pp. 4216-4219, November 2012.

[7] N. Velly, N. Takorabet, B. Nahidmobarakeh and F. Meibody-Tabar, "Calculation of radial forces in surface PM motors with assymmetric stator windings", International Conference on Electrical Machines (ICEM), pp. 2806-2811, September 2012.

[8] J. Le Besnerais, "Vibroacoustic analysis of radial and tangential air-gap magnetic forces in permanent magnet synchronous machines", *IEEE Trans. on Magn.*, vol. 51, no. 6, 8105609, June 2015.

[9] P. La Delfa, M. Hecquet, F. Gillon and J. Le Besnerais, "Analysis of radial force harmonics in PMSM responsible for electromagnetic noise", International Conference on Ecological Vehicles and Renewable Energies (EVER), pp. 1-6, April 2015.

[10] D.Y. Kim, J.K. Nam and G.H. Jang, "Reduction of magnetically induced vibration of a Spoke-Type IPM motor using magnetomechanical coupled analysis and optimization", *IEEE Trans. on Magn.*, vol. 49, no. 9, pp. 5097-5105, September 2013.

[11] S. Jia, R. Qu, J. Li, Z. Fu, H. Chen and L. Wu, "Analysis of FSCW SPM servo motor with static, dynamic and mixed eccentricity in aspects of radial force and vibration", Energy Conversion Congress and Exposition (ECCE), pp. 1745-1753, September 2014.

[12] K. Boughrara, R. Ibtiouen, and T. Lubin, "Analytical Prediction of Magnetic Field in Parallel Double Excitation and Spoke-Type Permanent-Magnet Machines Accounting for Tooth-Tips and Shape of Polar Pieces ", *IEEE Trans. on Magn.*, vol. 48, no. 7, pp. 2121-2137, July 2012.

[13] K. Boughrara, T. Lubin, R. Ibtiouen, and N. Benallal, "Analytical calculation of parallel double excitation and spoke-type permanent-magnet motors; simplified versus exact model," *Progress In Electromagnetics Research B*, Vol. 47, 145-178, 2013.

[14] M. Huo, S. Wang, J. Xiu and S. Cao, "Effect of magnet/slot combination on triple-frequency magnetic force and vibration of permanent magnet motors", Journal of Sound and Vibration, Elsevier, vol. 332, pp. 5965-5980, 2013.

[15] F. Dubas, and A. Rahideh, "2-D analytical PM eddy-current loss calculations in slotless PMSM equipped with surface-inset magnets", *IEEE Trans. on Magn.*, vol. 50, no. 3, 6300320, March 2014.

[16] D.C. Meeker, Finite Element Method Magnetics. ver. 4.2 (1 Apr. 2009 Build) [Online]. Available: http://www.femm.info

VI. Biographies

Kamel Boughrara was born Algiers, Algeria, in 1969. He received the Engineer Diploma from Ecole Nationale Polytechnique Algiers, Algeria, and the magister degree from the University of Sciences and Technology Houari Boumediene, Algiers, Algeria, in 1994 and 1997, respectively, and the Doctorat d'Etat degree from Ecolle National Polytechnique, Algeria, in 2008.

He is currently a Lecturer at Ecole Nationale Polytechnique (ENP, Algeria, at the Laboratoire de Recherche en Electrotechique (LRE-ENP). His interests include modeling and control of electrical machines.

Rachid Ibtiouen received the Ph.D. degree in electrical engineering from Ecole Nationale Polytechnique (ENP), Algiers, Algeria, and the Institut National Polytechnique de Lorraine, Nancy, France, in 1992.

He was with the Groupe de Recherche en Electrotechnique et Electronique de Nancy, Nancy, from 1988 to 1993. From 1993 to 2011, he was an Expert Member of the Committee of Evaluation of the University Projects of Research with the Comité National d'Evaluation et de Programmation de la Recherche Universitaire, Ministry of the Algerian Higher Education. From 205 to 2013, he was the Director of the Laboratoire de Recherche en Electrotechnique with ENP. He is currently a Professor and the Associate Director of Research with ENP. He is also the Head of the Department of Electrical Engineering with ENP. His current research interests include the modeling electric systems and drives, and, in particular, electrical machines.

Frédéric Dubas was born in Vesoul, France, in 1978. He received the Degree from the University of Franche-Comté (UFC), Belfort, France, in 2002, and the Ph.D. degree from the UFC, in 2006, with a focus on the design and the optimization of high-speed surface-mounted permanent-magnet (PM) motor for the drive of a fuel cell air-compressor.

He is currently an Associate Professor with the ENERGY Department, FEMTO-ST Institute, UFC where he is the Head of the "Unconventional Thermal and Electrical Machines" Team. He is with ALSTOM Transports, Ornans, France, and RENAULT Technocenter, Guyancourt, France, where he is involved in the modeling, design and optimization of electrical systems and, in particular, induction and PM synchronous (radial and/or axial flux) machines, creative problem solving, and electrical propulsion/traction. He has authored over 50 refereed publications and a patent about the manufacturing of axial-flux PM machines with flux-focusing.

Dr. Dubas received the Prize Paper Awards in the IEEE Conference Vehicle Power and Propulsion (VPPC) in 2005.